ACS APPLIED MATERIALS & INTERFACES

www.acsami.org

Research Article

Preventing Catastrophic Failure of Microfibrillar Adhesives in Compliant Systems Based on Statistical Analysis of Adhesive Strength

René Hensel,* Jonathan Thiemecke, and Jamie A. Booth*

Cite This: *ACS Appl. Mater. Interfaces* 2021, 13, 19422−19429

Read Online

ACCESS | Metrics & More | Article Recommendations

ABSTRACT: Adhesives based on fibrillar surface microstructures have shown great potential for handling applications requiring strong, reversible, and switchable adhesion. Recently, the importance of the statistical distribution of adhesive strength of individual fibrils in controlling the overall performance was revealed. Strength variations physically correspond to different interfacial defect sizes, which, among other factors, are related to surface roughness. For analysis of the strength distribution, Weibull's statistical theory of fracture was introduced. In this study, the importance of the statistical properties in controlling the stability of attachment is explored. Considering the compliance of the loading system, we develop a stability criterion based on the Weibull statistical parameters. It is shown that when the distribution in fibril adhesive strength is narrow, the global strength is higher but unstable detachment is more likely. Experimental variation of the loading system compliance for a specimen of differing statistical properties shows a transition to unstable detachment at low system stiffness, in good agreement with the theoretical stability map. This map serves to inform the design of gripper compliance, when coupled with statistical analysis of strength on the target surface of interest. Such a treatment could prevent catastrophic failure by spontaneous detachment of an object from an adhesive gripper.

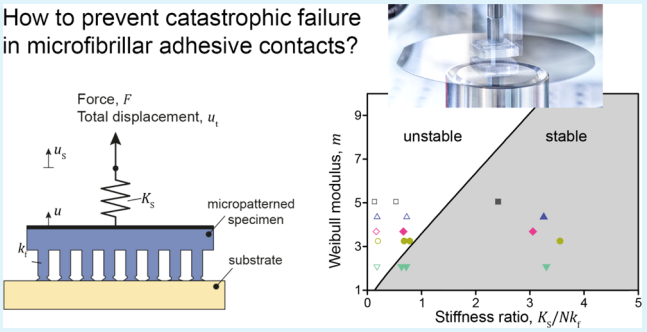

KEYWORDS: *adhesion, microfibrillar adhesives, Weibull statistics, system compliance, attachment stability*

1. INTRODUCTION

There has been significant recent progress in the development of high-performance and switchable microfibrillar dry adhesives.[1−4] The new technology enables reliable handling of delicate objects under various environmental conditions and can be easily integrated into automated grippers.[5−9] As the underlying adhesion mechanism is mainly based on van der Waals interactions, microfibrillar adhesives work similarly in air and under reduced air pressure.[10−12] As detachment must be initiated at each individual fibril, the work to separate the contact is typically larger than for a nonpatterned smooth adhesive.[13−15]

The diameter of synthetic fibrils is commonly on the order of several tens of microns. Therefore, adhesion failure is typically associated with critical defects at the interface between microfibril tips and the target surface. Detachment occurs via the propagation of these defects through the interface as the local load supported by a fibril reaches a critical value.[15] According to linear elastic fracture mechanics, for a compliant fibril adhered to a much stiffer substrate, the adhesion force has the general form

$$f_{max} = \beta\left(\frac{EW}{\pi a}\right)^{1/2} \quad (1)$$

where E is the elastic modulus of the fibril, W is the work of adhesion, a is the characteristic size of the critical defect, and β is a shape factor, which is a function of the geometric properties of the fibril and defect. Interfacial defects can result from manufacturing imperfections, dust, and surface roughness, and consequently vary in size and location within the contacting area at the fibril tip. As a result, and in accordance with eq 1, the adhesive strength of individual fibrils within a microfibrillar specimen varies.[10,16] In a previous report, we have demonstrated that the Weibull statistics can be used to describe the strength distribution.[17] This statistical approach is analogous to the

Received: January 15, 2021
Accepted: March 31, 2021
Published: April 13, 2021

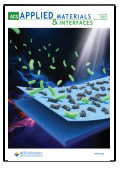

modeling of the ultimate strength of bundles of threads[18] and fiber-reinforced composites,[19,20] and provides characteristic measures, such as the Weibull modulus m, for the quantitative comparison of microfibrillar specimens.

The implementation of microfibrillar adhesives in grippers adds a stiffness component K_s (i.e., the stiffness of the loading system) in series with that of the microfibril array. Previous reports have shown that variation of the system stiffness affects crack propagation rates during debonding and, more significantly, can induce a transition from stable to unstable crack growth leading to catastrophic failure of the adhesive contact.[21,22] The stability criterion of adhesive contacts based on fracture mechanics was first introduced by Maugis.[23] We adapt this concept for the study of microfibrillar adhesives. The total displacement of adhesive and loading system relative to the substrate in the unloaded state is u_t, hence

$$u_t = u_s + u \tag{2}$$

where u_s is the loading system displacement and u is the displacement of the adhesive (Figure 1a). The total load supported by the specimen is

$$F = \sum_{i=1}^{N_a} f_i \tag{3}$$

where f_i is the load supported by an arbitrary fibril of the microfibrillar adhesive and N_a is the number of attached fibrils. If the load distribution is approximately uniform, this leads to

$$F = N_a f \tag{4}$$

where f is the local load supported by each fibril. Alternatively

$$F = N_a k_f u \tag{5}$$

where k_f is the stiffness of an individual fibril. Note that the assumption of a uniform load distribution is only correct for negligible backing layer compliance or very small array sizes. Deformable backing layers give rise to an array-edge load concentration, the details of which depend on the array size, fibril areal density, and fibril stiffness.[24,25] In previous work on equivalent microfibrillar samples as considered here, with identical backing layer thickness and array size, uniform load sharing was verified as no correlation was observed between the detachment of one fibril and that of its neighbors.[17] We also note that a nonuniform load distribution among fibrils is not expected to affect the qualitative trends observed in this work.

The stiffness k_f is assumed to be constant among fibrils in the array, and independent of displacement, i.e., each fibril responds in a linear elastic manner. Defect propagation at the fibril tip is assumed to occur in an unstable manner when the local load reaches a critical value, $f = f_{max}$, leading to the force–displacement response of an individual fibril shown in Figure 1b. Orange symbols represent a typical single-fibril experiment, and the black solid line the idealized response utilized in subsequent modeling. As fibril detachments occur, the total force supported will drop in accordance with eq 4. Instantaneously (i.e., at fixed total displacement u_t) the deformation of the loading system is reduced. This must be accommodated by a corresponding increase in the deformation of the adhesive according to

$$du = -dF/K_s \tag{6}$$

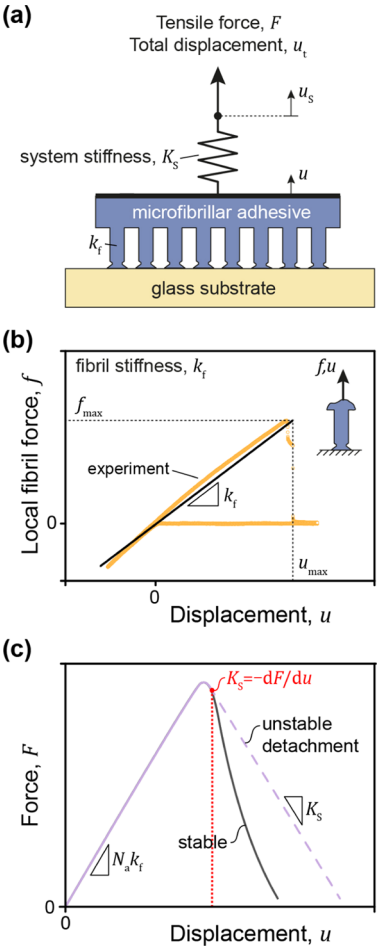

Figure 1. Schematic illustrating an adhesion test using a compliant system. (a) Schematic of the adhesion setup where the microfibrillar adhesive (blue) adheres to a nominally flat glass substrate (yellow). The force F and the total displacement u_t are recorded during tests. The applied load is shared by the attached fibrils N_a, which individually have stiffness k_f. The spring attached in series with the microfibrillar adhesive represents the loading system stiffness K_s. (b) Idealized (black solid line) and experimental (orange symbols) force–displacement curve of an individual fibril, with the adhesion force f_{max} and the elongation at detachment u_{max}. (c) Schematic of two force–displacement curves: The solid dark gray line represents stable detachment for a sufficiently stiff system fulfilling eq 9 throughout the detachment process. The purple line represents an exemplary experiment with lower system stiffness. The point of instability (red dot) occurs at the first instance at which $K_s = -dF/du$. Ongoing detachment is unstable (purple dashed line).

Rearranging this equation, it becomes apparent that during a detachment event the gradient of the force–displacement curve is controlled by the stiffness of the system

$$K_s = -dF/du \tag{7}$$

where necessarily

$$dF/du < 0 \tag{8}$$

as detachment triggers a drop in the load. If $-dF/du$ is greater than the stiffness of the system, then an instability will be triggered. In this situation, the system compliance dictates that the increase in displacement of the adhesive during a detachment event (eq 6) triggers further detachment events. In handling applications, this leads to catastrophic failure as the object would spontaneously detach from the gripper. Con-

https://doi.org/10.1021/acsami.1c00978
ACS Appl. Mater. Interfaces 2021, 13, 19422−19429

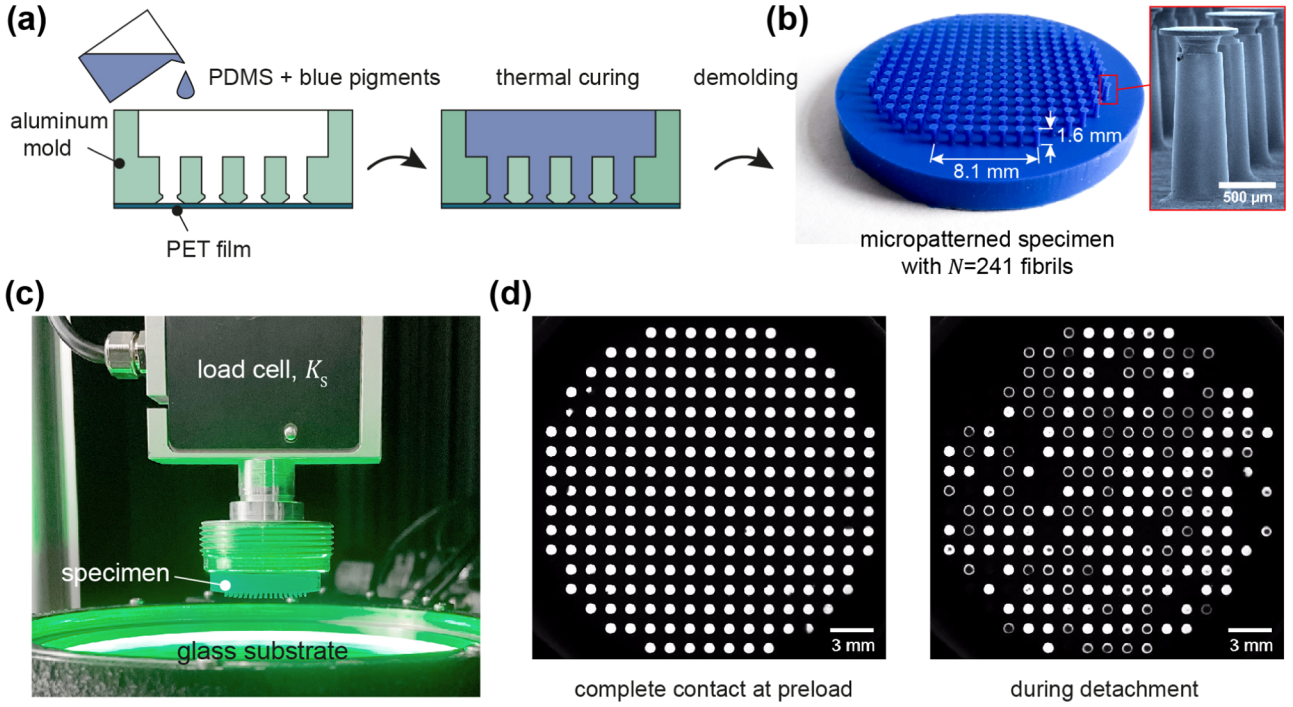

Figure 2. Fabrication of microfibril dry adhesives. (a) Schematic of replica molding where polydimethylsiloxane (PDMS) containing 10% blue pigments is poured into a micromachined aluminum mold. The bottom of the mold is covered with a polyethylene terephthalate (PET) film to close the holes. (b) Optical image showing the dimensions of the microfibrillar adhesive upon thermal curing and demolding. Scanning electron micrograph (inset) shows the mushroom-shaped fibrils in a side view. (c) Image of the experimental setup. (d) In situ observation of fibril contacts from below the substrate at preload (left) and during detachment (right). Light and dark areas represent contact and noncontact regions, respectively.

sequently, eqs 7 and 8 represent conditions for the onset of an instability when dF/du is the gradient observed in a displacement-controlled measurement. We note that Maugis equivalently arrives at this stability criterion by consideration of energy exchange in the system.[23] To avoid this scenario, the stiffness of the system must be such that the condition

$$K_s > -dF/du \tag{9}$$

is satisfied throughout the separation process as the load is reduced (eq 8). To illustrate this, Figure 1c shows the force–displacement curve associated with stable detachment in a stiff measurement system (dark gray solid line), where the condition of eq 9 is satisfied at all points. Also shown is a measurement in a compliant system, exhibiting an instability at the first point at which eqs 7 and 8 are satisfied (purple dashed line).

In the present work, the stability criterion is extended through consideration of the strength distribution of the fibrils within a microfibrillar specimen. To validate the model, we perform adhesion experiments with specimens exhibiting various degrees of roughness and imperfections using different system stiffnesses. Overall, we provide a stability map to predict unstable and stable detachment as a function of statistical properties of the adhesive strength for the specimen, along with the stiffness of the loading system and adhesive.

2. MATERIALS AND METHODS

2.1. Fabrication of Microfibrillar Dry Adhesives. Microfibrillar dry adhesives were replicated from polydimethylsiloxane (PDMS, Sylgard 184, Dow Corning, Midland, MI) using a microfibrillar aluminum mold as illustrated in Figure 2, and described earlier.[10,16] The mold contained microscopic holes, which were the negative of the mushroom-shaped micropillars. To induce variation in the adhesive strength of the microfibrils, the bottom of the mold was covered by different rough polyethylene terephthalate (PET) films. The roughness of the films was transferred to the mushroom caps as described in our previous report.[16] PET films were Melinex 401 CW (DuPont, Neu Isenburg, Germany) and Sigma (SIG GmbH, Düsseldorf, Germany). The former film was mechanically clamped onto the mold with a flat aluminum plate and the latter was thermally bonded at 120 °C to the mold. The PDMS was mixed in a ratio of base and curing agent 10:1. For better optical contrast, 10 wt % blue pigments (PK 5091, Degussa, Essen Germany) were added to the prepolymer. All components were mixed with 2350 rpm and degassed at 1 mbar for 3 min using a SpeedMixer (DAC600.2 VAC-P, Hauschild Engineering, Hamm, Germany). The prepolymer mixture was filled into the mold and degassed for 5 min at 1 mbar. Subsequently, the prepolymer was cured either at 75 °C for 2 h (specimens #2 and #5) or at 95 °C for 1 h (specimens #1, #3, and #4). Each specimen consisted of $N = 241$ microfibrils that were arranged in a square lattice with center-to-center distances of 1.35 mm (Figure 2b). The 1.6 mm long mushroom-shaped fibrils exhibited cap and stalk diameters of 700 and 400 μm, respectively (see inset in Figure 2b).

2.2. Adhesion Tests. Adhesion tests were performed with a tensile tester equipped with a 200 N load cell (Inspekt table BLUE, Hegewald & Peschke, Nossen, Germany), see Figure 2c. The system stiffness, K_s = 935 N mm^{-1}, was deduced from the slope of the force–displacement curve during unloading in the compressive regime. To emulate softer systems, springs of differing stiffness were added in turn between the specimen and the load cell (see Figure 3). The resulting stiffnesses of the system with the different springs in place were 7.9, 27.3, 32.7, 144, and 600 N mm^{-1}. The target substrate for adhesion measurements was a smooth, nominally flat glass substrate (10 mm thick, heat-resistant borosilicate TEMPAX float, MISUMI Europa GmbH, Frankfurt, Germany). Alignment of specimens with the substrate was realized by a $\theta - \phi$ goniometer (MOGO, Owis, Staufen im Breisgau, Germany). Specimens approached the substrate at a rate of 1 mm min^{-1} until a compressive preload of 2–2.7 N was reached. After preloading, the specimens were immediately withdrawn at a rate of 1 mm min^{-1} until the compressive force fell to zero. They were then retracted with a rate of 10 mm min^{-1} until the specimens fully separated from the substrate.

https://doi.org/10.1021/acsami.1c00978
ACS Appl. Mater. Interfaces 2021, 13, 19422–19429

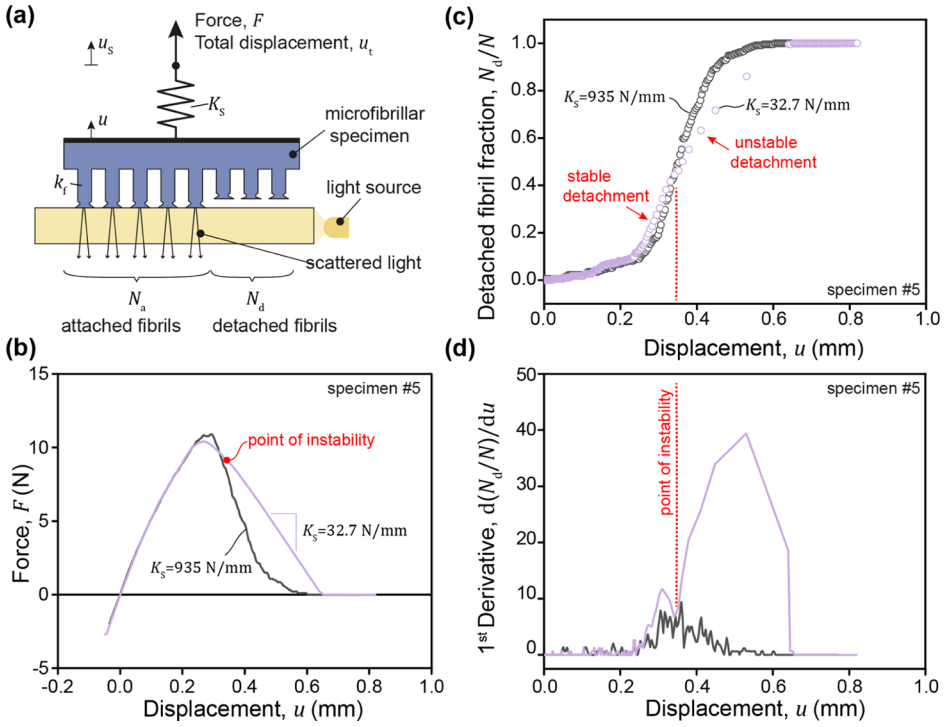

Figure 3. Adhesion tests and in situ observation of the detachment. (a) Schematic of the adhesion setup described in Section 2. The contrast between adhered and detached fibrils was enhanced by the principle frustrated total internal reflection, allowing the number of attached fibrils, N_a, to be determined by in situ visualization using a camera positioned under the substrate. The number of detached fibrils, $N_d = N - N_a$, where $N = 241$ is the total number of fibrils. (b) Force−displacement characteristics (F versus u) for specimen #5, testing using two different system stiffnesses, $K_s = 935$ N/mm (dark gray) and $K_s = 32.7$ N/mm (purple). (c) Fraction of fibrils detached from the substrate N_d/N versus the displacement of the adhesive u, for the testing of specimen #5 with both a stiff system, $K_s = 935$ N/mm (dark gray circles), and a soft system, $K_s = 32.7$ N/mm (purple circles). In the case of the soft system, the red dashed line highlights a sharp increase in the slope (i.e., the first derivative shown in (d)). This corresponds to the point of transition from stable to unstable detachment.

During the tests, the displacement of the motorized stage, the force on the load cell, and the time were recorded. To account for the elastic deformation of the loading system, the displacement of the adhesive, u, was calculated as follows: $u = u_t - F/K_s$, where u_t is the displacement of the motorized stage, F is the force normal to the interface (positive in tension) and K_s is the machine stiffness (see eq 1). Weibull moduli m, reference displacement u_0, and the stiffness of the fibrillar specimens Nk_f, were determined from experiments using the stiffest system, i.e., the 200 N load cell with $K_s = 935$ N mm^{-1}. All experiments were performed in a laboratory with regulated temperature and relative humidity at 21 ± 0.2 °C and 50 ± 5%.

2.3. Contact Visualization and Image Analysis. To detect fibril attachment, the optical contrast was enhanced by the principle of frustrated total reflection, as illustrated in Figure 3a. Light was coupled into the substrate such that it was only scattered when adhesive contact was established.[10,16,26] As a result, attached fibrils appeared as bright spots in bright-field illumination, whereas detached fibrils and the gaps between the fibrils were dark (Figure 2d). Formation and detachment of contacts were recorded with 50 frames per second (DMK33GX236, Imaging Source Europe GmbH, Bremen, Germany). Frames were binarized to determine the contact area and location (x-, y-coordinates) of the centroid of each fibril tip using the Computer Vision and the Image Processing toolboxes in MATLAB (MathWorks, MA). Locations were then correlated with forces and displacements from adhesion tests, whereas, for synchronization, the time step at which the last fibril detached from the substrate was attributed to the moment at which the tensile force dropped to zero.

3. RESULTS AND DISCUSSION

Figure 3a illustrates the adhesion tests, described in detail in Section 2, where the microfibrillar adhesive adhered to a nominally flat smooth glass substrate. Figure 3b displays example curves for force versus displacement of the adhesive that were obtained from two different system stiffnesses, K_s = 935 N/mm (dark gray) and K_s = 32.7 N/mm (purple). A maximum force of $F_{max} = 10.4$ N was attained at $u = 0.27$ mm for the soft system. For the stiffer system, the maximum force was slightly higher at $F_{max} = 10.9$ N, attained at $u = 0.29$ mm. The two curves deviate significantly at the point at which the negative gradient is equal to the stiffness of the softer loading system. This is a characteristic of unstable detachment, as introduced in Section 1 and Figure 1.

To confirm this, in situ observations of the progression of the detachment were utilized. Figure 3c displays the fraction of fibrils detached from the substrate N_d/N versus displacement of the adhesive u. This confirms that for the stiff loading system (K_s = 935 N/mm, dark gray) there is gradual detachment of a small subset of fibrils throughout the range of applied displacement. The soft system (K_s = 32.7 N/mm, purple), on the other hand, exhibits rapid detachment of approximately 60% of fibrils when a critical displacement of 0.34 mm was reached. This event (red dotted line) was accompanied by a rapid increase of the first derivative of the detached fibril fraction $d(N_d/N)/du$, as depicted in Figure 3d.

These results also demonstrate that the local force required to trigger detachment of each fibril varied throughout the array. For the stiff system, the first fibril of the array detached at a displacement of 0.05 mm and the last fibril at 0.60 mm (Figure 3c). Multiplying these values by the fibril stiffness k_f reported in Table 1 gives that the weakest adhesion force of an individual fibril is 12.2 mN and the strongest is 146.6 mN. For the soft

https://doi.org/10.1021/acsami.1c00978
ACS Appl. Mater. Interfaces 2021, 13, 19422−19429

Table 1. Properties of Microfibrillar Specimens Prepared with Differing Characteristics of Tip Roughness, as Described in Section 2.1[a]

specimen	Weibull modulus m	displacement u_0 (mm)	stiffness Nk_f (N/mm)
#1	2.0	0.325	44.0
#2	3.3	0.284	40.4
#3	3.6	0.294	47.1
#4	4.4	0.793	43.2
#5	5.1	0.381	58.9

[a]Characteristic statistical parameters m and u_0 are obtained from fitting (eq 10), as shown in Figure 4. The system stiffness was K_s = 935 N/mm for all measurements. Stiffnesses of the specimen were determined in the compression regime of force−displacement curves.

system, the first fibril of the array detached at a total displacement of 0.04 mm and the last fibril at 0.65 mm, which correspond to adhesion forces of 11.0 and 158.8 mN for the weakest and strongest fibrils, respectively. The observation of statistical variation is in agreement with previous studies of similar microfibrillar adhesives.[10,16,17]

Seeking to characterize this statistical variation, it is assumed that the adhesive strength of individual fibrils is uniquely related to the size and location of defects at the interface. Defect characteristics may differ from fibril to fibril within the array on account of surface asperities, roughness, chemical inhomogeneities, dust, fabrication imperfections, and so on. Under these conditions, it has been shown that the distribution of strength follows from Weibull's statistical theory of fracture.[17] The adhesive strength of a fibril can be described via the critical force for detachment (or adhesion force), as in eq 1. Equivalently, by invoking the stiffness of the fibril, it can be described using the elongation of a fibril at detachment, $u_{max} = f_{max}/k_f$. Proceeding with the latter for convenience, the detachment probability (i.e., the fraction of fibrils detached from the substrate) at an applied displacement of the adhesive u is given by the cumulative distribution function

$$\Phi = N_d/N = 1 - \exp\left[-\left(\frac{u}{u_0}\right)^m\right] \tag{10}$$

where u_0 is a reference value for the elongation of a fibril at detachment, related to the mean value according to

$$\bar{u}_0 = u_0\Gamma\left(\frac{1}{m} + 1\right) \tag{11}$$

where Γ is the γ function. The γ function term varies between 0.88 and 1 over the entire physical range of m from 1 to infinity. The Weibull modulus is a measure of the variability of the elongation at detachment and thus of the adhesive strength from fibril to fibril, with m = 1 representing the stochastic limit and m = ∞ the deterministic limit. For the latter, the elongation at detachment is u_0 for all structures. Figure 4 shows the theoretical fraction of fibrils detached from the substrate, N_d/N, versus normalized displacement u/u_0, for a fibril array exhibiting ideally Weibull distributed adhesive strength (inset), alongside equivalent experimental results for the five microfibrillar specimens used in the study (which have differing characteristics of tip roughness, as described in Section 2.1 and our previous reports[10,16]).

To obtain specific measures of m and u_0 for the five microfibrillar specimens used in the study, experimental values

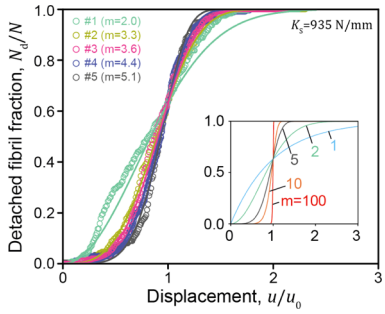

Figure 4. Fraction of fibrils detached from the substrate N_d/N versus normalized displacement u/u_0 (circles). The system stiffness was K_s = 935 N/mm. Solid lines correspond to best fits using eq 10 with parameters m and u_0 summarized in Table 1. The inset shows theoretical variations of N_d/N versus u/u_0 for Weibull moduli ranging from 1 (stochastic limit) to 100.

were extracted by fitting of eq 10 (solid lines in Figure 4). The values of m and u_0 are summarized in Table 1. We note here that instabilities can distort the shape of the N_d/N versus u curve (see Figure 3c), and thus stability must be ensured to accurately determine values of m and u_0. The highest possible system stiffness (K_s = 935 N/mm) was therefore chosen for determination of these statistical properties. No evidence of instability was observed in force−displacement or in situ observation data. Furthermore, given that the system stiffness is approximately 20 times that of the fibrillar specimens (N_ak_f = 46.7 ± 7.2 N/mm, see Table 1), the measurements are retroactively determined to be well within the stability boundary based on subsequent analysis (see eq 15 and Figure 7). The Weibull moduli ranged from 2.0 to 5.1 for the different microfibrillar specimens.

Substituting the detachment probability given in eq 10 into 5 provides the load in terms of the displacement of the microfibrillar specimens, as

$$F = N \exp\left[-\left(\frac{u}{u_0}\right)^m\right]k_f u \tag{12}$$

The result of eq 12 provides the force−displacement response of microfibrillar adhesives with ideally Weibull distributed adhesive strength as they are loaded to complete separation. Figure 5 shows the normalized force F/Nf_0 versus normalized displace-

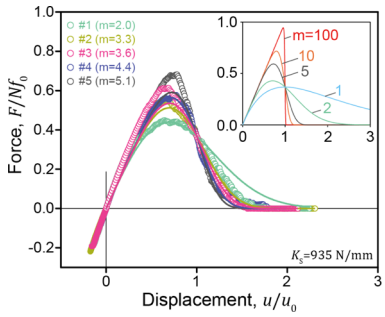

Figure 5. Normalized force F/Nf_0 versus normalized displacement u/u_0 obtained from adhesion tests (circles). The variable used for normalization of the force $f_0 = k_f u_0$. The system stiffness was K_s = 935 N/mm. Solid lines correspond to theoretical predictions given by eq 12 and the Weibull modulus of each specimen reported in Table 1. The inset shows characteristic force−displacement curves for Weibull moduli ranging from 1 (stochastic limit) to 100.

https://doi.org/10.1021/acsami.1c00978
ACS Appl. Mater. Interfaces 2021, 13, 19422−19429

Table 2. Comparison of Experimental and Theoretical Values[a]

specimen (Weibull modulus)	max. force, $(F/Nf_0)_{max}$		detached fibril fraction at instability, $(N_d/N)_c$ for K_s = 7.9 N/mm		detached fibril fraction at instability, $(N_d/N)_c$ for K_s = 32.7 N/mm	
	experiments	model	experiments	model	experiments	model
#1 (m = 2.0)	0.45	0.44	0.54	0.50	stable	stable
#2 (m = 3.3)	0.54	0.51	0.56	0.33	stable	0.6
#3 (m = 3.6)	0.61	0.53	0.56	0.30	stable	0.48
#4 (m = 4.4)	0.57	0.56	0.48	0.25	0.52	0.4
#5 (m = 5.1)	0.68	0.59	0.48	0.21	0.44	0.3

[a]Normalized maximum forces $(F/Nf_0)_{max}$, where $f_0 = k_f u_0$ (see Table 1), are calculated using eq 10. The fraction of fibrils detached from the substrate at the point of instability is calculated by combining eqs 10 and 13.

ment u/u_0 for experimental adhesion testing of the five microfibrillar specimens, alongside the theoretical prediction of eq 12 for the fitted values of m and u_0 obtained previously (Figure 4 and Table 1). The variable used for normalization of the force $f_0 = k_f u_0$. It should be emphasized that the determination of the statistical parameters by fitting relies only on the detached fibril fraction data (an optical measurement) and the displacement read-out from experiment, and thus the statistical parameters are completely independent of the force data, which are subsequently used to predict. These theoretical predictions show reasonable agreement with the experiments. Predicted maximum forces were slightly underestimated compared to the experiments, with deviations ranging from 1 to 15% (see Table 2). The inset in Figure 5 further highlights general theoretical trends on the maximum force $(F/Nf_0)_{max}$ and the shape of the curves in terms of m ranging between the stochastic (m = 1) and the deterministic ($m \to \infty$) limit. $(F/Nf_0)_{max}$ decreases from 0.95 (m = 100) to 0.37 (m = 1), whereas the shape of the curve simultaneously changes from a triangular shape with a drastic drop in force at u/u_0 = 1 to a shallow curve with a long tail and values of u/u_0 much larger than 1. This shows that a narrow distribution of fibril adhesive strength leads to a higher global strength, as fibrils reach their peak load close to simultaneously.

Having examined the force−displacement characteristics of separation, we return to the issue of stability. It is now apparent that the magnitude of the gradient dF/du when the load is decreasing, $dF/du < 0$, is dependent on the variability in fibril adhesive strength via the Weibull modulus (see eq 12 and Figure 5). Therefore, according to eq 9, the stiffness of the system required to ensure stability is also dependent on the variability in fibril strength. Taking the derivative of eq 12 with respect to the displacement, u, and combining with eq 9, we obtain the modified stability criterion

$$K_s > -Nk_f \exp\left[-\left(\frac{u}{u_0}\right)^m\right]\left[1 - m\left(\frac{u}{u_0}\right)^m\right] \quad (13)$$

which must be maintained across the entire range of displacement u for which the load is decreasing to ensure stable detachment. From Figure 5 (inset), it is apparent that larger Weibull moduli give rise to steeper gradients. That is, a narrow distribution of fibril adhesive strength will more readily give rise to an instability. With increasing Weibull modulus the critical gradients triggering instability will be encountered at lower displacements, and thus with a larger fraction of fibrils still in contact. The number of detached fibrils at the point of instability can be obtained by combination of eqs 10 and 13, when the latter has the inequality replaced with an equality.

Table 2 compares experimental observations with theoretical predictions of both the maximum force and the fraction of fibrils detached from the substrate at the point of instability. Figure 6

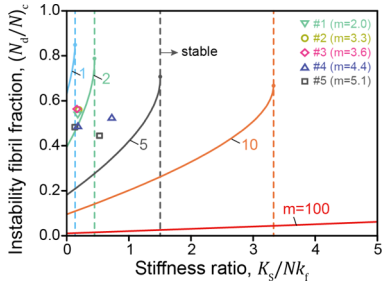

Figure 6. Fraction of detached fibrils at the point of instability $(N_d/N)_c$ versus stiffness ratio K_s/Nk_f. Solid lines represent the fibril fraction at the transition from stable to unstable detachment regimes, in terms of Weibull modulus m as given by eq 13. The dashed lines indicate the critical stiffness ratio above which the detachment is always stable. Symbols represent the experimental results for which unstable detachment was observed.

shows the fraction of fibrils detached from the substrate at the point of instability $(N_d/N)_c$ versus stiffness ratio K_s/Nk_f, for a range of Weibull moduli. The figure demonstrates that a larger variability of the adhesive strength among the fibrils (small m) affords stable detachment for softer systems (low K_s). In other words, a narrow distribution of fibril adhesive strength (large m) requires a stiffer system to avoid triggering an instability. Experiments confirmed unstable detachment (open symbols) for all specimens ($2.0 < m < 5.1$) tested with the softest system stiffness (K_s = 7.9 N/mm). For the next stiffest system (K_s = 32.7 N/mm), stable detachment was predicted for specimen 1 with m = 2.0 but, contrary to the theoretical prediction, was also stable for specimens #2 (m = 3.3) and #3 (m = 3.6). Unstable detachment was correctly predicted for specimens #4 (m = 4.4) and #5 (m = 5.1). As a general trend, the theoretical prediction underestimates $(N_d/N)_c$ for the two system stiffnesses (7.9 and 32.7 N/mm) that were considered in that comparison to the experiments. This may be related to the method by which $(N_d/N)_c$ was determined in experiment, from the displacement at which the last peak in the $d(N_d/N)/du$ versus u curve begins (see red dashed line in Figure 3c,d). Furthermore, $(N_d/N)_c$ greatly depends on the Weibull modulus when it is small (see steep gradients for low m in Figure 6), and thus the comparison between theory and experiment will be sensitive to error in the determination of m and u_0 by fitting.

The transition between stable and unstable detachment as the system stiffness is varied, always occurs when the gradient dF/du, as the load decreases, is most severe. Accordingly, we obtain

https://doi.org/10.1021/acsami.1c00978
ACS Appl. Mater. Interfaces 2021, 13, 19422−19429

the critical displacement associated with this transition by setting the second derivative of eq 12 with respect to the displacement u equal to zero. This yields

$$u_c = u_0\left[\frac{1}{m}(1+m)\right]^{1/m} \tag{14}$$

Replacing the inequality of eq 13 with an equality and substituting eq 14 provides

$$\left(\frac{K_s}{Nk_f}\right)_c = m\exp\left[-\frac{1}{m}(1+m)\right] \tag{15}$$

This equation describes the critical ratio of loading system stiffness to stiffness of the microfibrillar array at which transition between fully stable and unstable detachment occurs. Figure 7

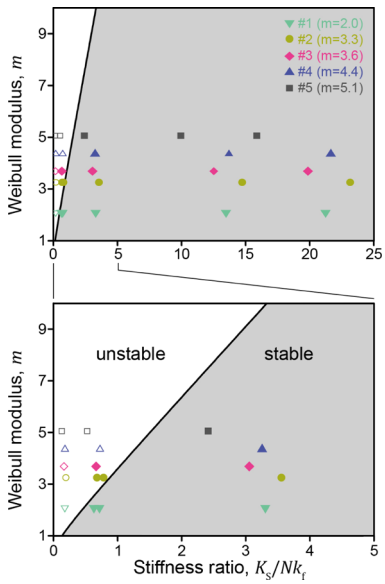

Figure 7. Map to predict stable (gray region) and unstable (white region) detachment as a function of Weibull modulus m and stiffness ratio K_s/Nk_f over the ranges $0 \le K_s/Nk_f \le 25$ (upper) and $0 \le K_s/Nk_f \le 5$ (lower). The solid line separating both regimes is given by eq 15. Symbols represent the experimental results, where full and open symbols correspond to stable and unstable detachment, respectively. The colors represent the specimens having various Weibull moduli m.

depicts the stability map based on eq 15. It shows good agreement with the experimental observations, except for three experiments near the transition line (specimens #2 and #3 and system stiffnesses of 27.3 and 32.7 N/mm). Overall, the results indicate that an increase in the variability of fibril adhesive strength, and thus the Weibull modulus, requires a stiffer loading system to maintain stable detachment.

4. CONCLUSIONS

The analysis and results presented above provide new insight into the performance of microfibrillar dry adhesives. In particular, we have demonstrated how a statistical variation in the local adhesive strength of individual fibrils and the compliance of the loading system alter the global adhesive strength and detachment characteristics. The following conclusions can be drawn:

- Parameters m and u_0, from Weibull's statistical theory of fracture, provide specific measures for each microfibrillar specimen that characterize the adhesive strength distribution among the fibrils as the characteristics of roughness at the interface are varied. Predicted force–displacement curves agreed with experimental results.
- When the force–displacement characteristics of separation of the micropatterned specimen and substrate are considered in combination with the stiffness of the loading system, a stability criterion for the detachment can be established. A narrow distribution in fibril adhesive strength, while providing a higher global strength, requires a stiffer loading system to ensure stability throughout detachment. The derived stability map was successfully validated by experiments. The map serves as a design guideline for the avoidance of unstable and therefore catastrophic detachment in handling delicate objects. Therefore, the stiffness of the gripping system relative to the micropatterned adhesive, as well as the statistical properties of the fibril adhesive strength on the target surface of interest, must be considered.

AUTHOR INFORMATION

Corresponding Authors

René Hensel − *INM—Leibniz Institute for New Materials, 66123 Saarbrücken, Germany;* orcid.org/0000-0002-9623-2118; Email: rene.hensel@leibniz-inm.de

Jamie A. Booth − *Mechanical Engineering Department, California State University, Northridge, California 91330, United States;* orcid.org/0000-0002-5171-667X; Email: jamie.booth@csun.edu

Author

Jonathan Thiemecke − *INM—Leibniz Institute for New Materials, 66123 Saarbrücken, Germany*

Complete contact information is available at: https://pubs.acs.org/10.1021/acsami.1c00978

Notes

The authors declare no competing financial interest.

ACKNOWLEDGMENTS

R.H. acknowledges partial funding by the Leibniz Competition Grant MUSIGAND (no. K279/2019).

REFERENCES

(1) Roberge, J.-P.; Ruotolo, W.; Duchaine, V.; Cutkosky, M. Improving Industrial Grippers With Adhesion-Controlled Friction. *IEEE Robot. Autom. Lett.* **2018**, *3*, 1041−1048.

(2) Song, S.; Drotlef, D.-M.; Majidi, C.; Sitti, M. Controllable Load Sharing for Soft Adhesive Interfaces on Three-Dimensional Surfaces. *Proc. Natl. Acad. Sci., U.S.A.* **2017**, *114*, E4344−E4353.

(3) Hensel, R.; Moh, K.; Arzt, E. Engineering Micropatterned Dry Adhesives: From Contact Theory to Handling Applications. *Adv. Funct. Mater.* **2018**, *28*, No. 1800865.

(4) Tinnemann, V.; Arzt, E.; Hensel, R. Switchable Double-Sided Micropatterned Adhesives for Selective Fixation and Detachment. *J. Mech. Phys. Solids* **2019**, *123*, 20−27.

(5) Cadirov, N.; Booth, J. A.; Turner, K. L.; Israelachvili, J. N. Influence of Humidity on Grip and Release Adhesion Mechanisms for Gecko-Inspired Microfibrillar Surfaces. *ACS Appl. Mater. Interfaces* **2017**, *9*, 14497−14505.

(6) Barreau, V.; Yu, D.; Hensel, R.; Arzt, E. Elevated Temperature Adhesion of Bioinspired Polymeric Micropatterns to Glass. *J. Mech. Behav. Biomed. Mater.* **2017**, *76*, 110−118.

(7) Heepe, L.; Kovalev, A. E.; Gorb, S. N. Direct Observation of Microcavitation in Underwater Adhesion of Mushroom-Shaped Adhesive Microstructure. *Beilstein J. Nanotechnol.* **2014**, *5*, 903−909.
(8) Barreau, V.; Hensel, R.; Guimard, N. K.; Ghatak, A.; McMeeking, R. M.; Arzt, E. Fibrillar Elastomeric Micropatterns Create Tunable Adhesion Even to Rough Surfaces. *Adv. Funct. Mater.* **2016**, *26*, 4687−4694.
(9) Arzt, E.; Quan, H.; McMeeking, R. M.; Hensel, R. Functional Surface Microstructures Inspired by Nature − From Adhesion and Wetting Principles to Sustainable New Devices. *Prog. Mater. Sci.* **2021**, No. 100778.
(10) Tinnemann, V.; Hernández, L.; Fischer, S. C. L.; Arzt, E.; Bennewitz, R.; Hensel, R. In Situ Observation Reveals Local Detachment Mechanisms and Suction Effects in Micropatterned Adhesives. *Adv. Funct. Mater.* **2019**, *29*, No. 1807713.
(11) Purtov, J.; Frensemeier, M.; Kroner, E. Switchable Adhesion in Vacuum Using Bio-Inspired Dry Adhesives. *ACS Appl. Mater. Interfaces* **2015**, *7*, 24127−24135.
(12) Sameoto, D.; Sharif, H.; Menon, C. Investigation of Low-Pressure Adhesion Performance of Mushroom Shaped Biomimetic Dry Adhesives. *J. Adhes. Sci. Technol.* **2012**, *26*, 2641−2652.
(13) Kamperman, M.; Kroner, E.; del Campo, A.; McMeeking, R. M.; Arzt, E. Functional Adhesive Surfaces with "Gecko" Effect: The Concept of Contact Splitting. *Adv. Eng. Mater.* **2010**, *12*, 335−348.
(14) Hui, C.-Y.; Glassmaker, N. J.; Tang, T.; Jagota, A. Design of Biomimetic Fibrillar Interfaces: 2. Mechanics of Enhanced Adhesion. *J. R. Soc. Interface* **2004**, *1*, 35−48.
(15) Zhang, X.; Wang, Y.; Hensel, R.; Arzt, E. A Design Strategy for Mushroom-Shaped Microfibrils With Optimized Dry Adhesion: Experiments and Finite Element Analyses. *J. Appl. Mech.* **2021**, *88*, No. 031015.
(16) Thiemecke, J.; Hensel, R. Contact Aging Enhances Adhesion of Micropatterned Silicone Adhesives to Glass Substrates. *Adv. Funct. Mater.* **2020**, *30*, No. 2005826.
(17) Booth, J. A.; Tinnemann, V.; Hensel, R.; Arzt, E.; McMeeking, R. M.; Foster, K. L. Statistical Properties of Defect-Dependent Detachment Strength in Bioinspired Dry Adhesives. *J. R. Soc. Interface* **2019**, *16*, No. 20190239.
(18) Daniels, H. E.; Jeffreys, H. The Statistical Theory of the Strength of Bundles of Threads. I. *Proc. R. Soc. London, Ser. A* **1945**, *183*, 405−435.
(19) Curtin, W. A.; Takeda, N. Tensile Strength of Fiber-Reinforced Composites: I. Model and Effects of Local Fiber Geometry. *J. Compos. Mater.* **1998**, *32*, 2042−2059.
(20) Zhou, S. J.; Curtin, W. A. Failure of Fiber Composites: A Lattice Green Function Model. *Acta Metall. Mater.* **1995**, *43*, 3093−3104.
(21) Barquins, M. Influence of the Stiffness of Testing Machines on the Adherence of Elastomers. *J. Appl. Polym. Sci.* **1983**, *28*, 2647−2657.
(22) Mojdehi, A. R.; Holmes, D. P.; Dillard, D. A. Revisiting the Generalized Scaling Law for Adhesion: Role of Compliance and Extension to Progressive Failure. *Soft Matter* **2017**, *13*, 7529−7536.
(23) Maugis, D. Adhesion of Solids: Mechanical Aspects. In *Modern Tribology Handbook*, Bhushan, B., Ed.; CRC Press, 2001.
(24) Bacca, M.; Booth, J. A.; Turner, K. L.; McMeeking, R. M. Load Sharing in Bioinspired Fibrillar Adhesives with Backing Layer Interactions and Interfacial Misalignment. *J. Mech. Phys. Solids* **2016**, *96*, 428−444.
(25) Booth, J. A.; Bacca, M.; McMeeking, R. M.; Foster, K. L. Benefit of Backing-Layer Compliance in Fibrillar Adhesive Patches-Resistance to Peel Propagation in the Presence of Interfacial Misalignment. *Adv. Mater. Interfaces* **2018**, *5*, No. 1800272.
(26) Samri, M.; Kossa, A.; Hensel, R. Effect of Subsurface Microstructures on Adhesion of Highly Confined Elastic Films. *J. Appl. Mech.* **2021**, *88*, No. 031009.

https://doi.org/10.1021/acsami.1c00978
ACS Appl. Mater. Interfaces 2021, 13, 19422−19429